Bispectrum-based Measurements of Close Large-Differential-Magnitude Visual Double Stars

J. Sérot
Clermont-Ferrand, France

Rick Wasson
Orange County Astronomers, Murrieta, California

Dave Rowe
PlaneWave Instruments, Rancho Dominguez, California

Russell Genet
California Polytechnic State University, San Luis Obispo, California

Abstract: This paper reports results of a collaborative project for assessing: (1) whether small-aperture telescopes might be used to collect reliable images of close visual double stars with large differential magnitudes (up to Δm=7) and faint late secondaries; and (2) whether bispectrum-based analysis techniques could be applied to the collected data in order not only to determine their position angles and separations, but also to obtain reliable estimations of differential magnitudes with different filters, with the ultimate objective of estimating the spectral type of the faint secondaries.

1. Introduction

Triple correlation (also known as bispectrum analysis) has been routinely used by professional astronomers in the field of close binary star observations (Horch *et al*. 2004). Relying upon speckle interferometry, this technique allows accurate measurements below the seeing limit. But, unlike classical auto-correlation-based analysis, it produces a fully reconstructed image of the observed pair. Therefore, in addition to identifying the correct quadrant of the secondary star, it also allows estimating the difference in magnitude (Δm) between the two components. Rowe has recently added a module performing bispectrum analysis to his *Speckle Toolbox* (STB) software (Harshaw, Rowe, and Genet, 2017) and experiments have shown that it can produce astrometric results on a par or better than those obtained with lucky imaging or auto-correlation (Sérot 2018b, Sérot 2018c). But these results are preliminary and, more importantly, do not address the issue of obtaining reliable estimations of Δm.

Obtaining reliable measurements of differential magnitudes for short-period visual binary stars is important, as it can provide information on the stellar types of the components and hence help in refining the models of stellar evolution. It is well known, in particular, that while the masses of stars in the middle of the main sequence are known with good accuracy from eclipsing binaries (Anderson 1991), this is not true for M-type stars. Dupuy *et al*. have shown that inferred masses for these stars can be off by a factor of two (Dupuy *et al.* 2012). A more direct, and potentially more accurate, way of computing these masses is to derive them from the orbit of binary stars. Close, short-period, visual double stars are good candidates for this because the separation between their components may be close enough to allow a significant portion of the orbit to be obtained in a relatively short period of time, but not so close (as with spectroscopic binaries for instance) that mass exchange affects their evolution.

There are two practical obstacles to the approach of using short-period visual binary stars with M-type companions for determining stellar masses. First, such pairs are difficult to observe because they generally exhibit small separation (usually below the atmospheric seeing

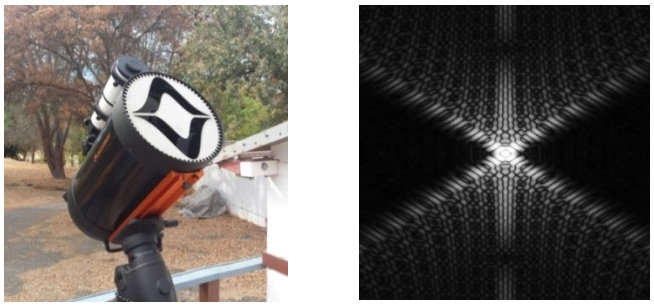

Figure 1. Foley's mask (left, here mounted on a C11 telescope) is based on the Spergel–Kasdin prolate-spheroidal mask originally described by Kasdin et al. (2003). It produces the diffraction pattern (right) plotted on a nonlinear brightness scale. Note the two triangular secondary star "discovery zones" that are relatively free of diffracted light from the primary star

limit for ground-based telescopes) and very large differential magnitudes (which implies that the light from the brighter star often overwhelms the light from the dimmer star). Second, of the many close double stars listed in the Washington Double Star (WDS) Catalog with large differential magnitudes (LDM), the spectral type of most of the secondaries is not known, primarily because it is difficult to determine using normal spectroscopic techniques. Thus, we don't know whether the secondary is a chance, more distant early star (and hence an optical double of little interest), or a nearby late star (a potential binary with a late-M star secondary and hence of great interest).

In late 2016, the authors embarked on a collaborative project for assessing whether small-aperture telescopes might be used to: (1) collect reliable images of close visual double stars with large differential magnitudes (up to $\Delta m=7$) and faint late secondaries, and (2) whether bispectrum-based analysis techniques could be applied to the collected data not only to determine (and follow) their position angles and separations, but to also obtain reliable estimations of differential magnitudes with different filters so that the spectral type of the faint secondaries could be roughly estimated. Because the available values for differential magnitudes were either lacking or imprecise (and because we had little previous experience with bispectrum reduction techniques) it was agreed to work on a common list of target stars to minimize, or at least identify, potential biases. Three observers were engaged in this campaign: R. Wasson (RW), J. Sérot (JS), and R. Harshaw (RH). The results reported in this paper are those obtained by RW and JS.

2. Previous and related work

As mentioned above, observing close doubles with large differential magnitude is challenging because the light from the bright primary simply swamps the light from the faint secondary. There are several ways this problem can be circumvented.

Shaped aperture masks can be used to diffract the bright light from the primary star away from "discovery zones," allowing faint secondaries to be observed. Many shaped masks have limited-angle discovery regions, so one must rotate these masks to fully survey the neighborhood of a star (Kasdin *et al.* 2003). Other mask species provide full 360-degree visibility around a star but do so at the expense of throughput or resolving power (Vanderbei *et al.* 2003). In general, larger discovery zones are associated with poorer contrast.

Other mask varieties have been proposed in the context of high-contrast imaging, including Lyot coronography and apodized masks. Lyot coronographs use a series of lenses and masks to isolate and remove centrally-incident light from the image (Sivaramakrishnan *et al*. 2001). These systems require accurate manufacturing techniques and precise positioning to function properly (Sing *et al*. 2013). Apodized masks, also called gradated masks, are used much like shaped aperture masks but feature a continuous transmission profile rather than either complete transparency or opaqueness. The smooth patterns theoretically can provide results superior to shaped aperture masks, but these results are difficult and expensive to achieve in practice.

Foley et al. (2015) developed a shaped aperture mask that shows some promise. While such a single, full-aperture, shaped pupil mask can help with large delta-mag close doubles, additional masks of various sorts can be placed at the image plane or Lyot stop. Adding such masks increases the degrees-of-freedom in the design space, which should allow a larger contrast ratio to be reached and therefore difference in magnitude. Although these additional masks would be much smaller, with tighter manufacturing and alignment tolerances, the contrast-ratios sufficient for double star research (approximately 10^2 to 10^3) are more modest than those for exoplanet imaging and so such additional masks may be within reach. There are a number of young giant planets (such as the HR 8799 system, to give the most famous example) that are within reach of 10^5 contrast, and have been imaged from the ground with AO systems at Keck, Palomar, and GPI (Gemini Planet Imager). A contrast ratio of 10^8 is the design figure being used for space-based science goals.

Another approach for easing the detection of close, late-M secondaries is to observe at longer wavelengths. This potentially reduces the light from an earlier primary while enhancing the light from the later secondary, thus reducing the differential magnitude. A short-wave

Figure 2. The OCA Kuhn 22-inch Cassegrain telescope instrumented for Speckle Interferometry. Camera, power, control and image acquisition are through the single blue USB3.0 cable to the laptop computer at lower right, running FireCapture software.

infrared (SWIR) InGaAs camera operating in the Y, J, and H bands (0.9-1.7μ) could work well. Sérot (2018a) has made a few initial observations with a Raptor Owl SWIR camera but the cost of these cameras still precludes their generalized use in the amateur community (though the situation may change in the very near future with the rapid development of a market for such cameras in the surveillance domain).

3. Instrumentation

The observations reported in this paper were conducted by two observers in two different locations : R. Wasson (RW) in Southern California and J. Sérot (JS) in France.

Wasson used a 22-inch classical Cassegrain telescope (Fig. 2), owned by the Orange County Astronomers astronomy club (OCA). This equipment, located at 4500 feet elevation in the foothills 15 miles east of Mount Palomar Observatory in Southern California, is described by Wasson (2018) and has been used for speckle interferometry since 2015. The results reported in this paper were obtained with a 2x Barlow lens and a

Figure 3. – Instrumental setup in Clermont-Ferrand. Left : C11 on equatorial mount. Right : optical train (flip mirror, centering eyepiece, filter wheel, projecting eyepiece and ADC – inside the tube between the filter wheel and the camera – and Raptor Kite EM-CCD

ZWO ASI290MM back-illuminated CMOS camera. The low-read-noise camera was not cooled; dark-subtraction processing would probably have improved the results but was not employed. The STB "interference" filter option was used in all processing, to suppress residual CMOS "read" noise, which otherwise causes a bright horizontal line through the images. No Atmospheric Dispersion Corrector (ADC) was used, restricting observations to zenith angles of less than about 35 degrees with moderate bandwidth near IF filters.

Because the back-illuminated CMOS camera has good QE in the near IR, an IR-pass filter (Astronomik Pro Planet 807) was used for observations of LDM pairs. It was assumed that when the primary star is a main sequence dwarf, a much fainter binary companion must be a later-type dwarf, most likely a late K or M dwarf. Therefore, the IR-pass filter was used for these initial observations. Even though the longer IR wavelength reduces the resolvable separation slightly, it should significantly reduce the magnitude difference and the required camera dynamic range.

Another benefit of near-IR observations is that the seeing is much better ("slower") than at shorter wavelengths, permitting longer exposures to record faint red stars. Exposures of 200 to 500 milliseconds were used by RW for these stars; this is about 10 times longer than usually achievable for visible wavelengths.

Sérot's observatory is located in the observer's garden at the periphery of Clermont-Ferrand, a mid-sized town in the center of France (45°47'N Lat., 3°04'E Long.) (Figure 3). The results reported in this paper

have been obtained using a Schmidt-Cassegrain reflector (Celestron C11) and a Raptor Kite EM-CCD camera (Sérot 2015, Sérot 2016a). The native focal length of the telescope (2.8 m, F/D=10) was augmented using 10 mm and 12 mm projecting eyepieces leading to pixel scales of 0.09''/pixel and 0.13''/pixel respectively. A wide-band L filter (400-700 nm) and exposures of 40-80 ms were used. An atmospheric dispersion corrector was inserted in the optical path to compensate for the effects of atmospheric dispersion.

4. Bispectrum analysis

Bispectrum analysis (BSA) – also known as triple-correlation – is an extension of the auto-correlation (AC) technique which has been used by professional astronomers for many years and is now used by several amateurs to obtain astrometric measurements of double stars below the seeing limit†.

Classical AC-based analysis operates by computing and summing the power spectrum of the images in the input sequence (taking the square of the modulus of the Fourier transform of each image) and then computing the inverse Fourier transform of the sum. In the resulting image, called an *auto-correlogram*, each secondary component gives two identical and symmetric peaks, located 180° apart from the central peak corresponding to the primary component. This technique works remarkably well for recovering the full resolution of an instrument, especially when used in conjunction with a deconvolution process, which reduces the effect of the *seeing halo* by dividing the accumulated power spectrum by that obtained for a single reference star under the same conditions.

Auto-correlograms, however, have two inherent limitations. First, since each companion gives two identical peaks in the auto-correlogram, there is always a 180° uncertainty in the measured position angle (known as the "quadrant ambiguity problem"). This is not a problem when the position of the companion is already known, at least approximately (from orbit ephemerids for instance) but is problematic for stars with few previous observations. Second, and more importantly in the context of this paper, the auto-correlogram does not allow estimation of the differential magnitude of the double star, because the intensity of the auto-correlation peaks is not related to the actual magnitudes of the components.

Bispectrum analysis (BSA) aims at overcoming the limitations of AC-based techniques. Technically, the *bispectrum* of an image is a four-dimensional complex matrix embodying the triple correlation of this image. Unlike the simple auto-correlation, the bispectrum retains the complex amplitude and hence makes it possible to recover the original image phase in the Fourier domain that is lost when the power spectrum is computed by squaring the modulus of the Fourier amplitude (as with auto-correlation). In practice, the final image phase is calculated from the bispectrum by an iterative procedure; the complex Fourier amplitude of the final image is calculated from the square root of the power spectrum, and the phase determined from the bispectrum. This allows a representation of the original set of images to be reconstructed with atmospheric distortion removed.

As with simple AC techniques, BSA is more effective when used with a reference (single) star. The power spectrum and bispectrum are computed for the reference star and are then used to compensate the power spectrum and bispectrum of the target double star.

The latest version of the Speckle ToolBox software (1.13) contains the modules necessary to reconstruct the image using BSA. The work described in this paper partly served as a test bench to assess the provided functions. The procedure is executed in two steps. One first constructs the bispectrum from the average of the triple correlation of each image in the ensemble. This process is computationally intensive, typically taking 10 times more CPU time than the computation of the power spectrum alone. The second step is the reconstruction of the final image from the power spectrum and bispectrum. This step, which iterates the image phase until convergence, is usually quite fast. During this step, the user can apply filters and photon bias removal in the Fourier domain to improve the SNR of the final image.

5. Targets

The eleven observed stars are listed in Table 1 with their characteristics obtained from the WDS catalog (Mason *et al.*, 2015). Columns 1-2 give the star identification (WDS number and discoverer code, respectively). Columns 3, 4, and 5 give the year of the first and last measurement and the total number of measurements. Columns 6-9 give the measurement values (PA=position angle in degrees, SEP=angular separation in arcsec) for the first (1) and last (2) measurement. Columns 10-12 give the magnitudes of the two components (Johnson V band is typical in WDS) and the corresponding ΔM value. Column 13 gives the spectral type of the primary component. Unfortunately, for the

† *AC-based reduction techniques are often referred to as "speckle interferometry" though, strictly speaking, the latter term should only be used when the acquired images show a sufficiently high number of fully resolved speckles, which only happens in practice for high D/R0 ratios. For small instruments, the technique should rather be called pixel auto-autocorrelation because the correlation is computed on raw pixels instead of speckles, which are either absent or too faint*

Table 1 – List of Target Stars Observed

WDS	DISC	DATE1	DATE2	NOBS	PA1	PA2	SEP1	SEP2	M1	M2	DM	SP
13122+1608	A 2225	1910	1997	7	69	74	3.0	2.5	7.52	13	5.48	F3V
14046+3425	HU 646	1903	2010	4	26	24	2.0	2.2	8.05	14.5	6.45	A3IV
14122+4225	HO 57	1883	2014	8	207	204	1.8	2.7	8.2	13.2	5.0	K5
14171+5433	BU 1271	1892	1996	13	355	355	2.8	1.8	7.1	12.3	5.2	G1IV
14525+2348	COU 305	1968	1998	3	66	66	3.2	3.6	7.37	12.5	5.13	K0
15190+2541	LDS6304	1960	2007	2	185	191	4.0	3.6	7.96	13.7	5.74	G8V
15483+1400	A 1637	1907	1975	4	256	257	2.2	2.8	9.69	14.9	5.21	K2
15536+1604	A 2079	1909	1991	6	61	59	3.5	3.4	6.26	12.5	6.24	F3V
16315+3331	BU 816	1881	1998	18	224	222	5.0	4.6	7.12	12.2	5.08	A2V
16335+3030	BU 818	1881	2009	9	34	38	3.3	4.0	6.9	13.5	6.6	A9IV
16529+4608	A 1869	1908	1945	4	214	226	2.3	2.3	9.02	15.1	6.08	G0

selected stars, the spectral types of the companions are not listed in the WDS, probably because they have not been spectroscopically observable in the glare of the nearby primary star.

The selection was based upon the magnitude, separation, spectral types of the components (as published in the WDS), and the visibility from both observatories. As announced in the introduction, the most salient feature exhibited by these pairs is their high ΔM values (ranging from 5.0 to 6.6) and the relatively close separations (from 1.7 to 4.6 arcsec). As can be expected – because of the large reported ΔM – these pairs have not been measured often (less than 10 times, on average, since their discovery). Three of the target stars are subgiants (spectral class IV) according to the WDS. These primaries are much brighter than a dwarf of the same type. Therefore, the companion may not be a late-type dwarf, but could be a normal dwarf of any type.

6. Results

All targets were observed between May 24, 2017 and Jun 1, 2017 (mean date: 2017.397). Results are listed in Tables 2 and 3.

Table 2 gives, for each target, the measured values for the position angle PA and the separation SEP obtained by the two observers (RW and JS) using two reduction methods: classical auto-correlation (AC) and bispectrum analysis (BSA). All AC and BSA values were obtained using the STB software (version 1.12 and 1.13).

The post-reduction images, from which these measurements were obtained, are given in Plates 1-11. In these plates, the first and second column show the autocorrelogram (top) and bispectrum-reconstructed image (bottom), both computed by STB, by the two observers (col 1: RW, col 2: JS). The last column shows an image of the pair obtained using the classical *lucky stacking* (LS) method, *i.e.* by co-adding the 10-30 best images of the acquisition sequence. This image was obtained by JS using the Reduc software (version 5.03) from F. Losse (Losse, 2017).

Table 2 shows that for each observer, the AC and BSA techniques give very consistent astrometric results: the mean and standard deviation of the difference in PA and SEP are μ=-0.28°/σ = 0.23° and μ = 4 mas σ = 62 mas for JS, and μ = 0°/σ = 0.40° and μ = 1 mas σ = 24 mas for RW. Moreover, the results obtained by both observers for each method are also very consistent: the mean and standard deviation of the difference for PA and SEP are μ = -0.4°/σ = 0.72° and μ = 13 mas σ = 43 mas for AC and μ = -0.19°/σ = 0.78° and μ = 20 mas σ = 63 mas for BSA respectively.

Table 3 gives the measurements of the differential magnitude Δm (m2-m1) obtained by both observers from the bispectrum-reconstructed images (as shown in the second row of Plates 1-11) and also, for JS, from the lucky stacked images (LS, as shown in the last column of Plates 1-11).

The LS values were obtained using the *Surface* algorithm provided by *Reduc*, which operates by fitting a mathematical profile on the non-saturated images of the stars.

The BSA values were obtained with STB using the method classically used for photometric measurements on CCD images. The *Speckle ToolBox* software uses three circular apertures to measure differential magnitude of the two stars simultaneously: an aperture for the primary star, one for the secondary star, and one for the background. The background aperture is placed in a "dark" area, away from both stars, and its average pixel value is subtracted from every pixel within the two star apertures.

Image calibration by JS was limited to dark and bias subtraction, but no flat fielding was done. No cali-

Bispectrum-based Measurements of Close Large-Differential-Magnitude Visual Double Stars

Table 2 – Measurements (PA and SEP)

Target	PA (°)				SEP (arcsec)			
	AC		BSA		AC		BSA	
	JS	RW	JS	RW	JS	RW	JS	RW
A 2225	72.1	72.5	72.5	72.5	3.00	2.98	2.99	2.95
HU 646	22.7	25.0	23.5	25.8	2.10	2.06	2.06	2.08
HO 57	204.8	204.6	205.0	204.5	2.56	2.57	2.57	2.56
BU 1271	353.9	354.0	354.3	354.0	1.68	1.67	1.64	1.67
COU 305	64.8	65.2	64.8	64.6	3.70	3.72	3.70	3.67
LDS6304	157.5	157.6	157.6	157.6	3.24	3.32	3.34	3.33
A 1637	n/a	258.3	257.4	257.7	n/a	2.66	2.78	2.68
A 2079	61.2	60.7	61.3	60.6	4.00	3.97	4.03	4.00
BU 816	220.4	221.0	220.5	221.0	5.05	5.05	5.07	5.03
BU 818	36.1	36.2	36.4	36.3	4.17	4.11	4.02	4.14
A 1869	219.4	220.1	219.8	220.6	2.18	2.10	2.22	2.09

Table 3 – Measurements (Δm)

Target	**Δm**		
	JS (center WL 530nm)		**RW (center WL 885nm)**
	BSA	**LS**	**BSA**
A 2225	4.7	4.6	3.9
HU 646	4.2	3.7	2.6
HO 57	4.1	4.0	4.0
BU 1271	3.9	3.1	3.1
COU 305	5.2	5.3	4.7
LDS6304	5.2	5.2	3.3
A 1637	3.7	3.2	3.3
A 2079	6.3	6.2	4.7
BU 816	4.8	5.2	3.5
BU 818	6.2	7.2	5.3
A 1869	5.0	4.4	3.5

bration was made to the RW images.

For JS, the Δm values obtained from the bispectrum -reconstructed images on the one hand and the lucky stacked images on the other hand are reasonably consistent, with a difference showing a mean value of -0.10 and a standard deviation of 0.46.

The values obtained by both observers using the same BSA method differ more significantly, with a mean value of 0.95 and standard deviation of 0.60 for the difference. This is not surprising since each observer used a different camera-filter combination. JS used a broad band "L" filter ($\lambda c \approx 550$ nm, $\Delta\lambda \approx 300$ nm), while RW used an IR-pass filter and a camera with relatively higher QE in the 800-1050 nm range. Since no attempt was made to transform the reported "raw instrumental" magnitudes to a "standard" photometric system†, the conclusions drawn from the observations must be made with care. Rough comparisons can still be made, however. In Figure 4 the Δm values obtained by both observers using the BSA method are plotted against filter center wavelength. Also shown as colored bars are the approximate filter pass bands used by each observer. It might be noted that the magnitude difference is always smaller at longer wavelength, generally indicating that the secondary star is redder than the primary.

The spectral type of each star is noted in the legend, with early types at top of the legend, and later types at

†*Such a transformation would be difficult and uncertain, because of large differences (in both center wavelength and band width) from any standard photometric filter set.*

Table 4 - Filters Used for Multi-Band Observations of High-Delta-Magnitude Double Stars with the OCA 22" Cassegrain and ZWO ASI290MM CMOS Camera

Filter Code	Manufacturer	Name	Type	Center WL (nm)	50% Transmission (nm)
G	Baader	G (LRGB Series0	Interference	534	495 to 575
R	Baader	R (LRGB Series)	Interference	636	582 to 690
IR742	Astronomik	ProPlanet 742	Interference	844*	736 to *
IR807	Astronomik	ProPlanet 807	Interference	885*	800 to *
* Indicates long-pass filter. Wavelength cutoff is determined by camera Quantum Efficiency. "Center" wavelength is weighted average of filter transmission times camera QE.					

bottom. It should be noted that the spectral type is likely dominated by the primary star alone, because it is much brighter; it is very difficult to get a spectrum for a faint star without contamination from such a bright nearby companion. Indeed, no spectra apparently exist for the faint secondary stars. There is no consistent trend in the delta magnitude slopes (i.e., color difference) with spectral type. The three K stars – the reddest primaries – all have relatively "flat" delta magnitudes, indicating that the primary and secondary stars are both reddish. But other stars of similar spectral type are not so consistent.

6.1. Multi-band Observations

As an extension of the work presented here, two stars listed in Table 1 were observed again by RW in multiple filters with the OCA 22-inch telescope. The filters employed are shown in Table 4, where the "cutoff" wavelength of the IR-pass filters was assumed to be 1050 nm (the approximate end of response for the back-illuminated silicon CMOS detector). The "center" wavelength is the weighted average of filter transmission times detector QE.

The idea was to check whether faint companions can be observed at shorter wavelengths and, if so, how the observed Δm varies with wavelength. Filters on hand were used for this initial exploration. Results obtained from auto-correlation (STB 1.05) and bispectrum analysis (STB 1.13) are given in Table 5. The faint red companions, down to V = 13.7, were successfully observed in all filters, even the G filter (center 534 nm). The PA and Separation data are quite consistent for both stars; standard deviations are small, even combining all filters and both analysis methods. This confirms that the AC and Bispectrum techniques both give valid astrometric results independently of the observing

Table 5 - Results of Multi-Band Observations of High-Delta-Magnitude Double Stars with the OCA 22" Cassegrain and ZWO ASI290MM CMOS Camera, on date 13 July 2017 (2017.531)

Double Star					Θo (deg)		ρo (")		
WDS	Discovery	WDS (V) m1 / m2	WDS DMag	Filter	AC	BS	AC	BS	DMag
15190+2541	**LDS6304**	7.96/13.7	5.74	G	157.76	157.65	3.339	3.357	5.31
				R	157.76	158.51	3.341	3.292	4.50
				IR742	157.63	157.46	3.323	3.321	3.21
				IR807	157.56	157.43	3.326	3.327	3.08
Average					157.72		3.328		
Standard Deviation					0.34		0.019		
16315+3331	**BU816**	7.12/12.2	5.08	G	221.01	221.05	5.067	5.076	4.22
				R	220.94	221.03	5.062	5.071	3.75
				IR742	221.00	221.08	5.054	5.043	3.41
				IR807	221.05	221.11	5.048	5.034	2.90
Average					221.03		5.057		
Standard Deviation					0.05		0.015		

Bispectrum-based Measurements of Close Large-Differential-Magnitude Visual Double Stars

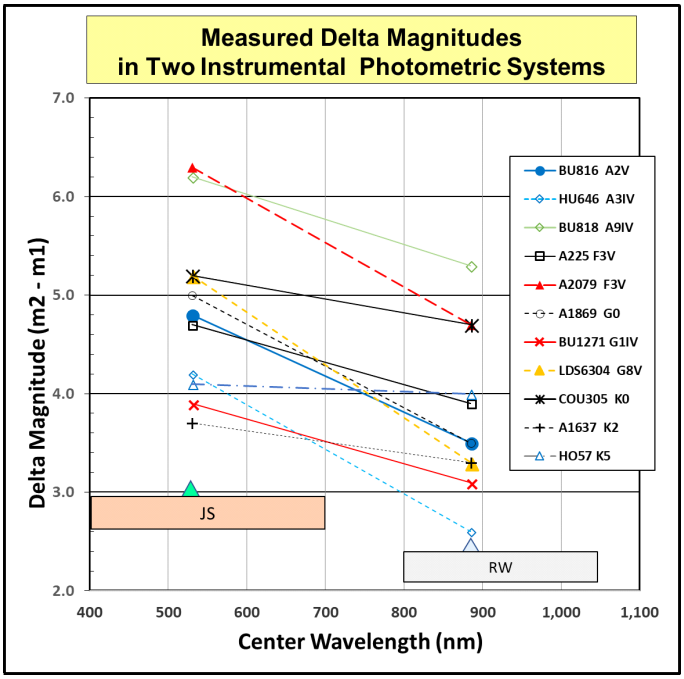

Figure 4. Measured Delta Magnitudes (Secondary – Primary) in two instrumental photometric systems.

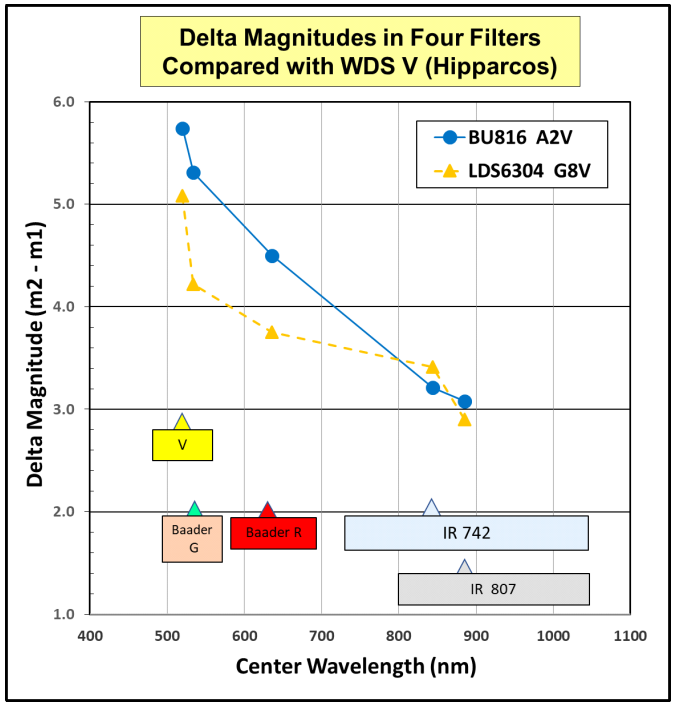

Figure 5. Measured Delta Magnitudes of two double Stars in four filters, compared with WDS V magnitudes.

wavelength.

The delta magnitude results of Bispectrum analysis are plotted in Figure 5 for the two stars observed. The bars at bottom indicate the filter passbands and center wavelengths. The left-most point and yellow bar indicate the WDS value, assumed to be the Johnson V band. There is a clear trend that the companion becomes relatively brighter (reduced delta magnitude) as wavelength increases, indicating that both secondary stars are quite red. The delta magnitude of the G filter approaches, but does not reach, that of WDS (V). The G filter is similar in center WL and 50% transmission to V; however, the G interference filter has sharp edges, without the red "tail" of the colored-glass V filter. No attempt was made to transform these magnitudes to a standard system.

In Figure 5, the early-type star BU816 (primary spectral type A2V) has a much steeper slope than the later-type star LDS6304 (primary type G8V). This trend would be expected if both secondary stars were of similar late spectral type, such as red dwarfs. This trend is also different from that in the previous comparison of Figure 4, where both stars had similar slopes. In Figures 4 and 5, the IR807 filter observations of RW were on different dates, and are shifted by about 0.4 magnitude. This could possibly be caused by variability in one or both stars, but more likely indicates uncertainty in measuring delta magnitude for such faint secondary stars. In Figure 4, the wide effective filter passband used by JS may also contribute to large differences in delta magnitude for different spectral types, because the dominant blue or red colors of the primary star can both be recorded, effectively shifting the "center" wavelength for each star.

6.2. Gaia Satellite Observations

The Gaia astrometric / photometric / radial velocity satellite, launched in late 2013, has completed a large portion of its planned observations. Exhaustive documentation is available on-line at http://sci.esa.int/gaia/. The second of four planned data releases - DR2 - became available to the public in April 2018. Although DR2 is a preliminary release, it contains a great deal of useful information having unprecedented accuracy (https://www.cosmos.esa.int/web/gaia/dr2).

Author Dave Rowe wrote code to download and access the 1.3 TB database. He then searched it for all stars in the WDS Catalog with separation less than 30", successfully identifying two components for over 76,000 doubles. Those with very high proper motion were difficult to locate. He built a file containing parameters of particular interest to double star observers; this file is in .csv spreadsheet format, for easy access, and is available for download by request.

Both components of all 11 double stars observed in

this paper were observed by Gaia, and DR2 parameters are summarized in Table 6. For each double, the first line is for the primary, and the second line for the secondary. The epoch of DR2 is given as 2015.5. The number of significant digits has been arbitrarily rounded to moderate precision in Table 6 - adequate for our purposes, but still much higher accuracy than heretofore available.

The columns of Table 6 contain the following data: WDS numerical designation, Discovery designation, Proper Motion in RA (milli-arcseconds/year), Proper Motion in Dec (milli-arcseconds/year), Parallax (milli-arcseconds), Distance (calculated from parallax, light-years), G, G_{BP}, and G_{RP} magnitudes, derived Radius (solar radii), derived Temperature (K), measured Radial Velocity (km/sec), derived Luminosity (sun=1), Separation (arcseconds), and Position Angle (degrees), both calculated from absolute position.

The G magnitudes are derived from the entire white light response (330-1050 nm) of the optics and astrometric CCD arrays, while G_{BP} (330-680 nm) and G_{RP} (640-1050 nm) magnitudes are the product of low-resolution spectrophotometer (prism) instrumentation (Pancino, 2010). A number of other parameters, not included in Table 6, are contained in DR2. But for any given star, some parameters may not be included, perhaps because sufficient analysis has not yet been performed.

A number of significant conclusions can be drawn from review of Table 6:

1. Based on very similar Proper Motion (direction and speed), Parallax (distance), and Radial Velocity (in only one case), the two components of each system are very near each other in space, and we conclude that all 11 double stars we observed are true binaries.
2. Unfortunately, because none is closer than 110 L-Y, their separation is several arcsec, and they have shown very little movement since discovery (4 to nearly 14 decades), they all probably have very long orbits.
3. All available prior observations were obtained courtesy of Brian Mason of the USNO. Some of these double stars were discovered over 100 years ago, but all have very few observations. Along with Gaia and the current observations, no systematic changes in separation or PA indicating orbital motion were seen.
4. Comparison of Tables 2 and 6 shows that our observations agree well with the Gaia separation and PA; the epochs are only about two years apart.
5. Gaia variability data were not available for any of the components; at this stage of the mission, variables may not have been evaluated in detail yet.

Table 6 - Summary of Preliminary Properties from Gaia Satellite DR2, Epoch 2015.5

WDS	Dicovery	PM RA (mas/yr)	PM Dec (mas/yr)	Parallax (mas)	Distance (l-y)	Gmag	BPmag	RPmag	Radius (sol)	Teff (K)	RV (km/s)	Lum (sol)	G Sep (")	G PA (deg)
13122+1608	**A2225**	-22.45	69.32	8.43	383	7.360	7.592	7.031	2.56	6673	-17.3	11.66	2.957	72.38
		-21.01	64.66	9.10	355	12.189	-	-	-	-	-	-		
14046+3425	**HU646**	-18.54	10.01	6.59	490	8.045	8.137	7.900	-	8157	-	-	2.087	23.80
		-16.99	10.59	6.63	487	11.882	-	-	-	-	-	-		
14122+4225	**HO57**	-38.54	-3.57	3.83	844	7.887	8.530	7.160	9.85	4697	-53.0	42.53	2.552	204.41
		-38.45	-2.69	3.58	903	11.971	-	10.303	-	-	-	-		
14171+5433	**BU1271**	-169.90	-57.35	19.18	168	6.836	7.219	6.332	2.09	5573	-45.6	3.79	1.697	353.24
		-168.55	-67.18	18.75	172	10.763	-	-	-	-	-	-		
14525+2348	**COU305**	-21.15	23.05	3.95	818	6.948	7.518	6.278	13.82	**4806**	-52.3	91.84	3.692	65.32
		-21.01	23.65	3.92	823	11.982	11.718	10.783	-	**5096**	-55.6	-		
15190+2541	**LDS6304**	-564.57	-125.14	29.42	110	7.798	8.198	7.272	0.94	5402	-30.9	0.676	3.330	158.41
		-544.13	-113.37	29.33	110	12.091	12.451	10.727	-	4947	-	-		
15483+1400	**A1637**	-1.52	-64.31	4.73	683	9.280	9.801	8.638	3.67	4941	-7.6	7.22	2.670	257.74
		-3.22	-64.74	5.53	584	12.736	13.164	11.804	0.69	4797	-	0.228		
15536+1604	**A2079**	20.20	-22.55	11.83	273	6.095	6.332	5.757	3.42	6513	-0.6	19.02	3.973	60.73
		20.19	-24.38	12.41	260	11.830	11.383	10.519	-	5096	-	-		
16315+3331	**BU816**	-25.28	-11.23	7.03	459	7.082	7.148	7.011	2.50	7982	-	22.94	5.044	221.08
		-20.47	-10.15	7.10	455	11.477	11.897	10.869	0.79	5173	-17.1	0.405		
16335+3030	**BU818**	-38.12	-2.79	5.79	558	6.818	6.959	6.624	3.71	7624	-	41.88	4.120	36.35
		-35.97	-3.83	5.93	545	12.681	12.566	11.749	-	5096	-	-		
16529+4608	**A1869**	1.95	-45.45	8.83	366	8.802	9.111	8.364	1.60	5924	3.8	2.85	2.139	221.34
		1.27	-43.97	8.75	369	12.995	-	-	-	-	-	-		

6. For those secondary stars that have Teff listed, the range is ~4800K to ~5200K. Based on the Gaia H-R diagram, using the (G_{BP} - G_{RP}) color index, this temperature range corresponds roughly to spectral types G8 through K2; therefore, these are apparently common dwarfs. None of these secondaries are red dwarfs (cooler than ~3800K), but later releases may include more red dwarfs.
7. The large Radius and Luminosity of several of the primary stars indicate that they are giants or subgiants.
8. In most binary systems, the secondary star is cooler than the primary, but the secondary star of COU305 is hotter. The cooler primary appears so much brighter (□G ~ 5) because it is likely a red giant, almost 14 times the size of the sun.

7. Discussion

While conducting the photometric measurements on the bispectrum-reconstructed images, several questions arose regarding the accuracy of the inferred values. This section summarizes these questions.

As stated in Sec. 6, estimation of the magnitude of each component is carried out using a small circular aperture centered around the component. A question naturally arising is how "small" this aperture should be.

In "classical", single star, photometry, the aperture size is generally simply chosen to include the seeing disk and exclude any other nearby star. For close double stars the situation is more complicated because the involved plate scales generally make the instrumental diffraction pattern – Airy disk and rings – apparent, as evidenced in Plates 1-11.

At first sight, and since the goal of photometry is to capture all the star's light in the aperture, it could seem that the bigger the aperture is the more accurate the measurement is. But large apertures create two problems. First, for faint stars, as the aperture increases, the background soon starts adding noise faster than captured starlight. Second, for very close stars, the diffraction rings of both components are overlapping, so that measuring the magnitude of a companion with an aperture too large may include some light from the bright primary star's rings.

This suggests using an aperture no bigger than the Airy disk. Using the Airy disk of the primary star for sizing the aperture appears reasonable. After all, the theory says that the angular diameter of this disk only depends on the telescope aperture and the observed wavelength and hence is the same for all stars in the same image. In practice, it appears smaller for faint stars because, in this case, only the central, brightest area emerges from the noisy background. This means that using an aperture derived from the Airy disk of the brightest component for measuring the faintest could lead to contamination by the background noise and/or the light of the primary.

As a result, we chose to size the measurement aperture using the image of the faintest star. In practice, we brighten the image until the background becomes visible, to identify the region where the faint star merges into it. And we use the same size aperture for the brightest star. This way we obviously measure *less than all* the light for both stars, but still the *same proportion* for each one.

An extra complication arises when the faint companion sits on (or partly on) a diffraction ring from the primary. In this case it will appear artificially brighter because of that contaminating light, making the delta magnitude smaller than it should be. To address that problem, we might, in the future, use a two-step sequence. First, the instrumental magnitude of the faint star alone could be obtained using the same size aperture for both star and background, but with the background located on the same ring nearby. Then the bright star could be measured in the usual way, with its background aperture in a dark region, to get its instrumental magnitude separately. The final measurement would be obtained by just taking the difference. We have not used this procedure yet. It might be a useful technique, but it is difficult to know whether it would really improve the accuracy of the differential magnitude.

8. Conclusion and Perspectives

The results reported in this paper confirm that bispectrum analysis, as supported by the latest versions of the *Speckle ToolBox* software, not only gives astrometric results on a par with those provided with autocorrelation based methods, but also solves the classical quadrant ambiguity problem.

Results for photometric measurements, in the case of large differential magnitudes pairs, are also encouraging, although requiring further investigation. Concerning the measurement process itself, the influence of the various noise sources and distortions on the shape of the reconstructed PSFs and, in turn, on the accuracy of the final measure remains to be quantified, as does the optimal aperture (in terms of a fraction of the Airy disk) used for measuring the individual magnitudes. The use of a standard photometric system (e.g., Johnson -Cousins or Sloan) may also be necessary to achieve more consistent and astro-physically meaningful results.

Automation of multi-band speckle interferometry

(Text continues on page 726)

Bispectrum-based Measurements of Close Large-Differential-Magnitude Visual Double Stars

AC	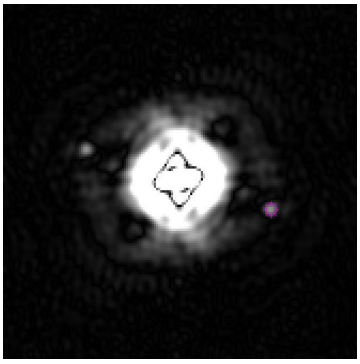	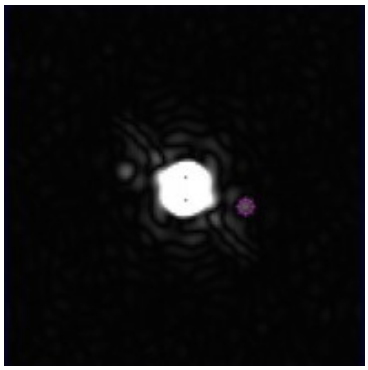	Plate 1 WDS 13122+1608 A 2225
BS	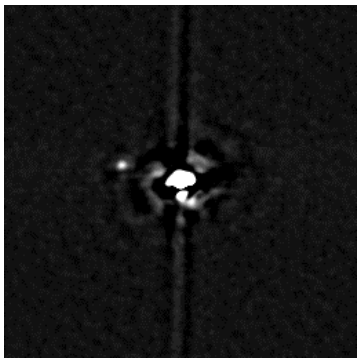	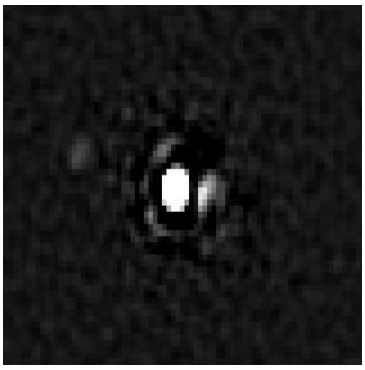	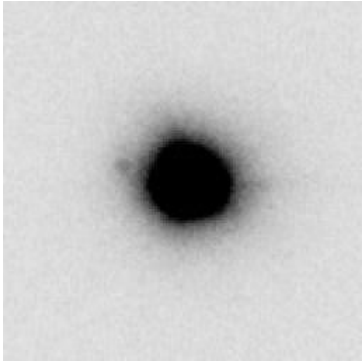
	RW	JS	LS

AC	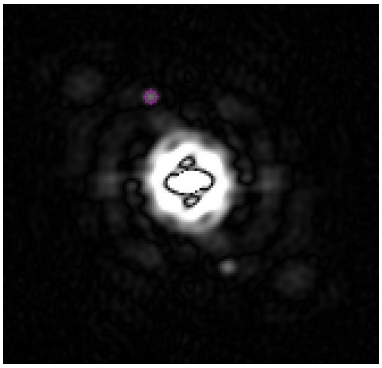	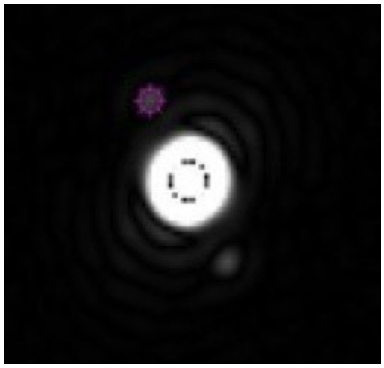	Plate 2 WDS 14122+4225 HO 57
BS	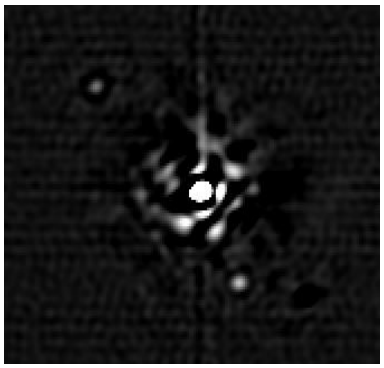	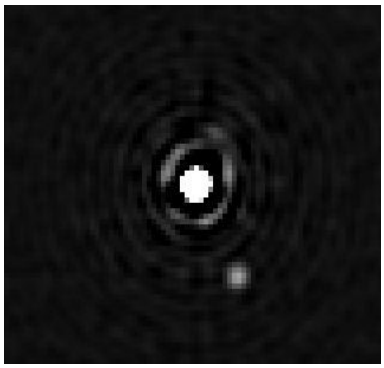	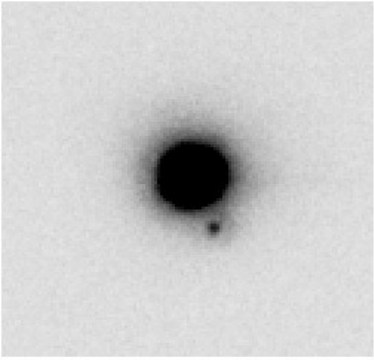
	RW	JS	LS

Bispectrum-based Measurements of Close Large-Differential-Magnitude Visual Double Stars

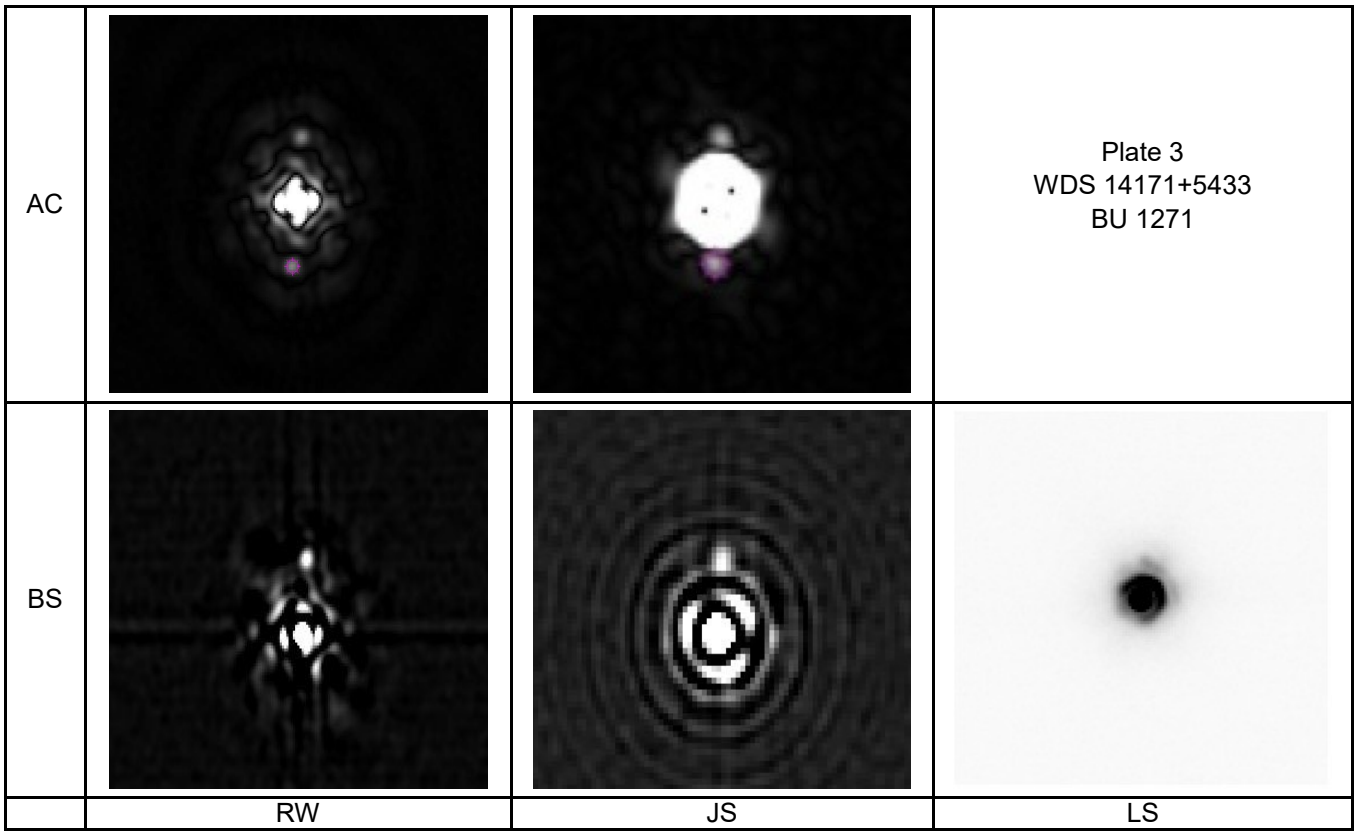

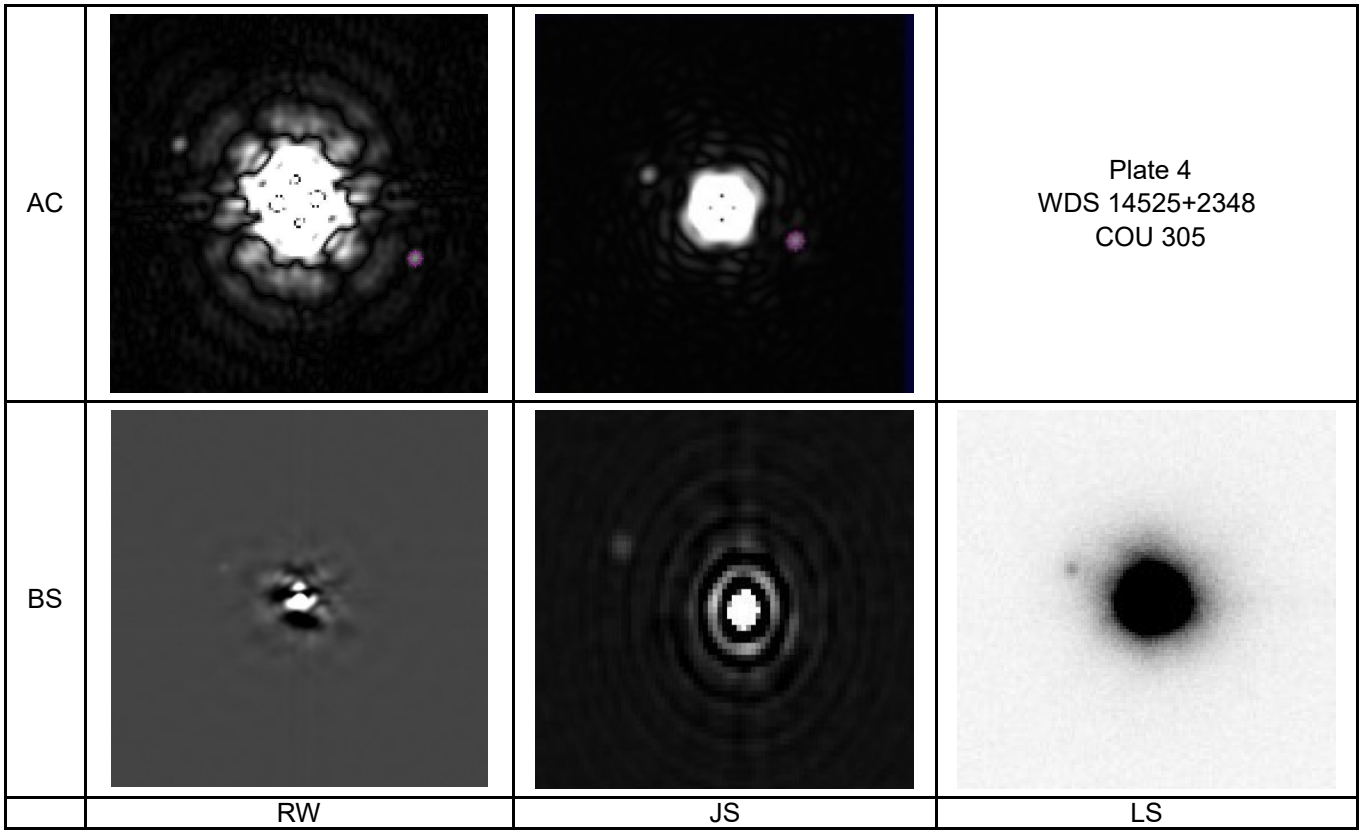

Bispectrum-based Measurements of Close Large-Differential-Magnitude Visual Double Stars

AC	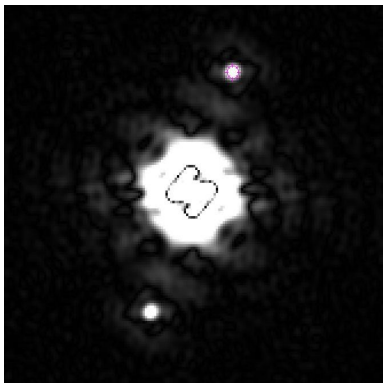	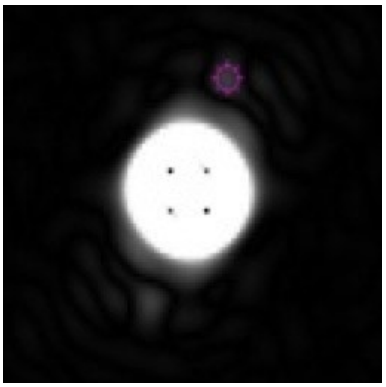	Plate 5 WDS 15190+2541 LDS6304
BS	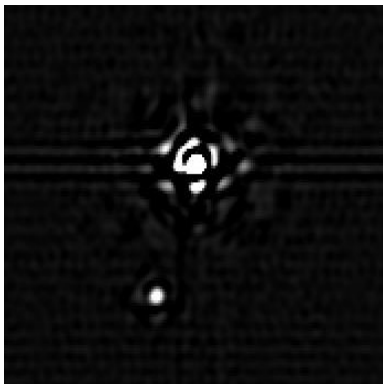	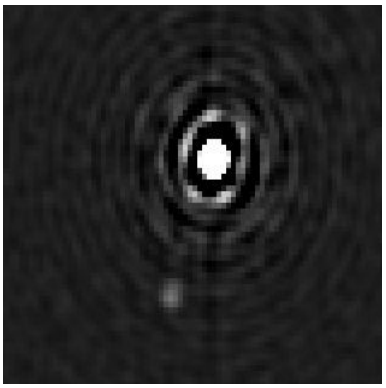	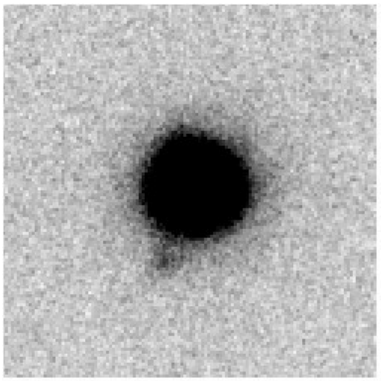
	RW	JS	LS
AC	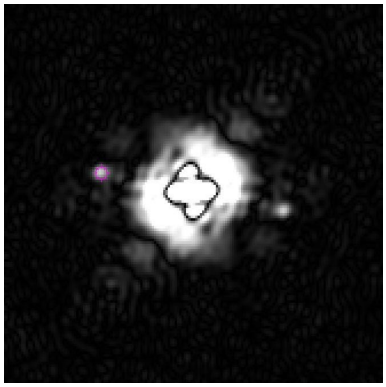	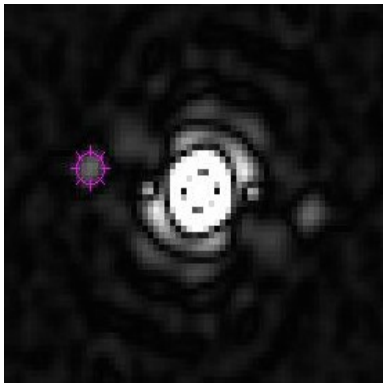	Plate 6 WDS 15483+1400 A 1637
BS	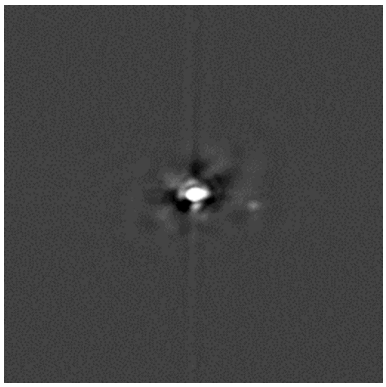	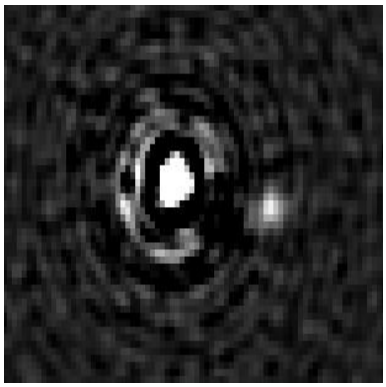	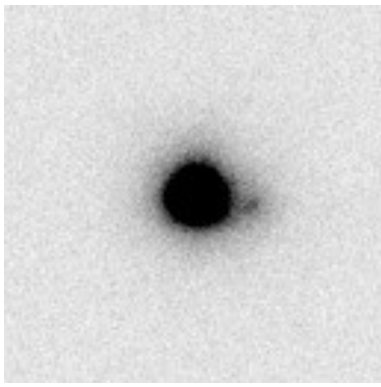
	RW	JS	LS

Bispectrum-based Measurements of Close Large-Differential-Magnitude Visual Double Stars

AC	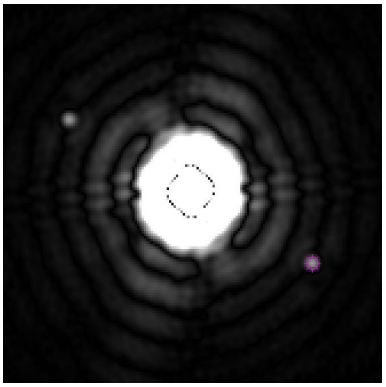	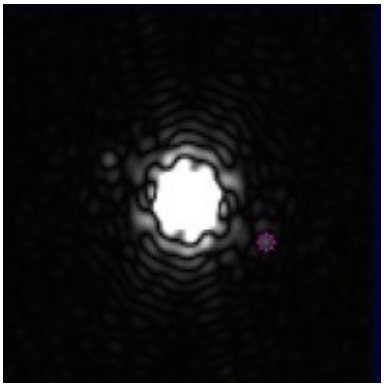	Plate 7 WDS 15536+1604 A 2079
BS	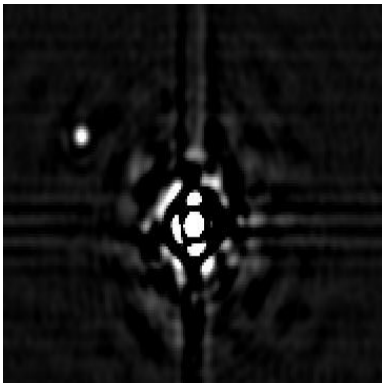	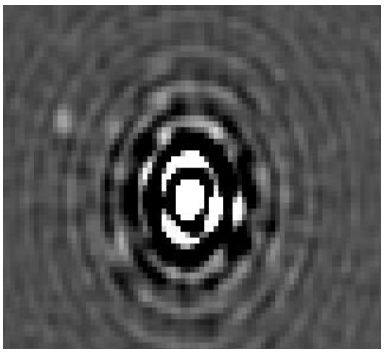	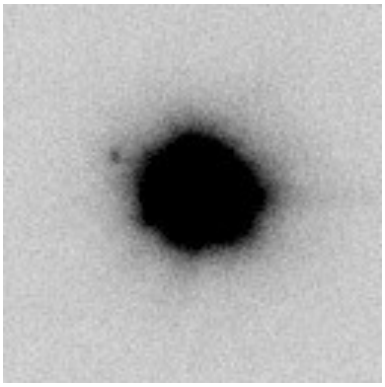
	RW	JS	LS

AC	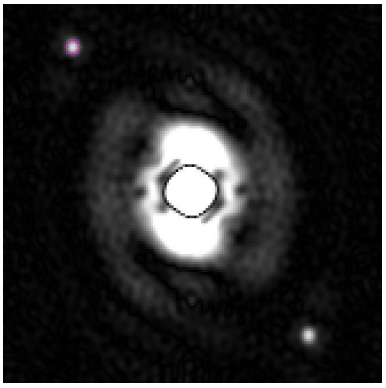	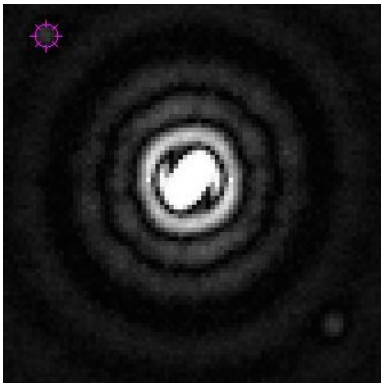	Plate 8 WDS 16315+3331 BU 816
BS	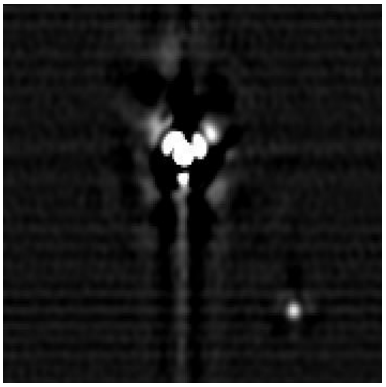	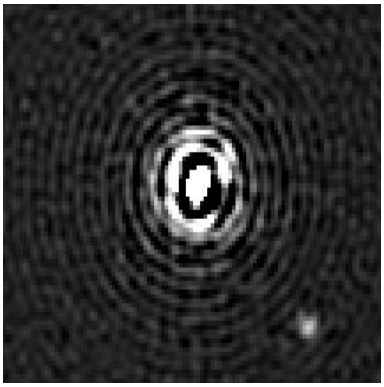	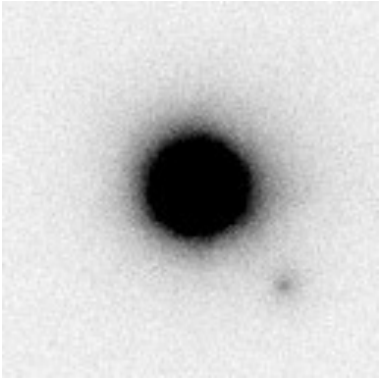
	RW	JS	LS

Bispectrum-based Measurements of Close Large-Differential-Magnitude Visual Double Stars

AC	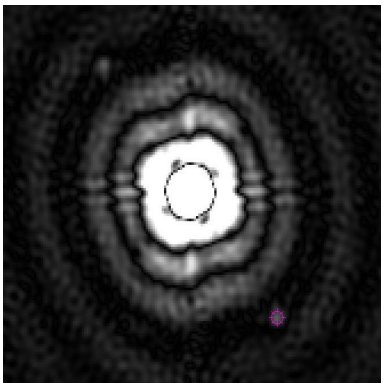	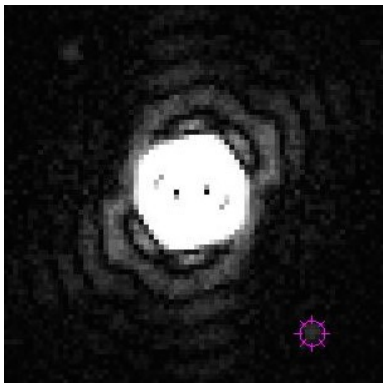	Plate 9 WDS 16335+3030 BU 818
BS	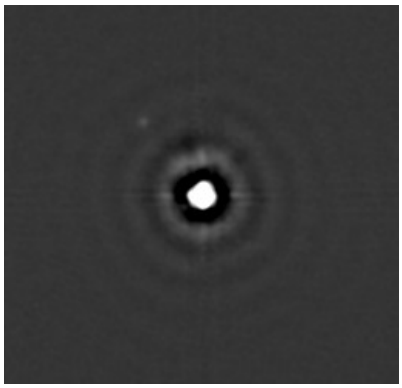	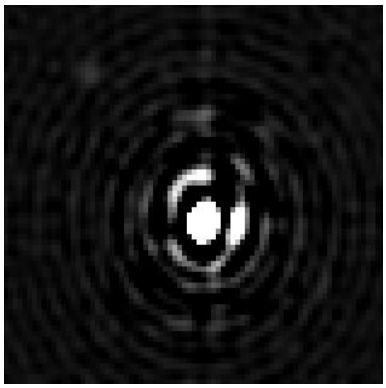	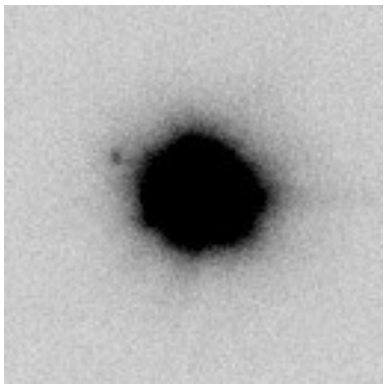
	RW	JS	LS

AC	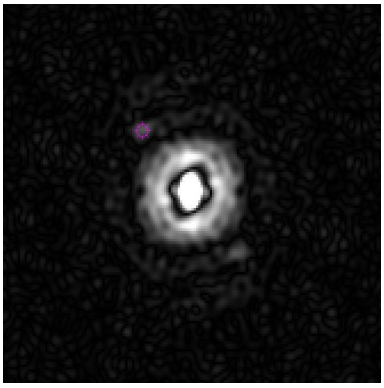	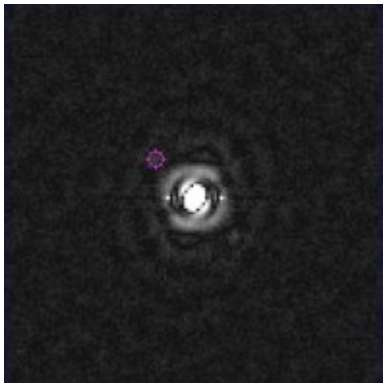	Plate 10 WDS 16529+4608 A 1869
BS	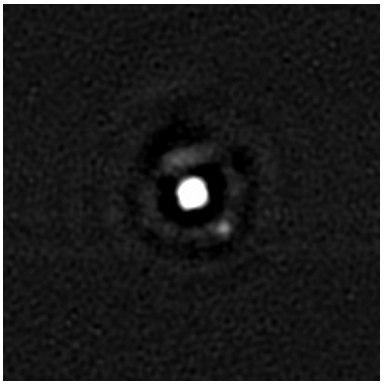	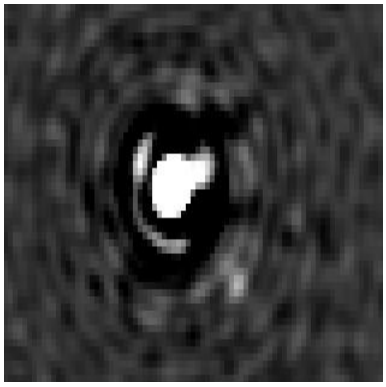	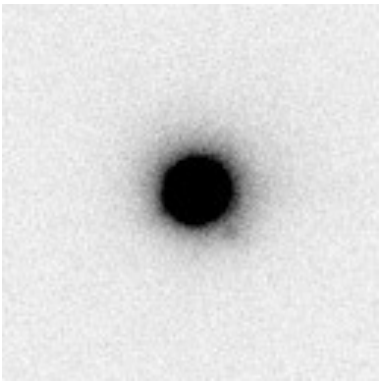
	RW	JS	LS

Bispectrum-based Measurements of Close Large-Differential-Magnitude Visual Double Stars

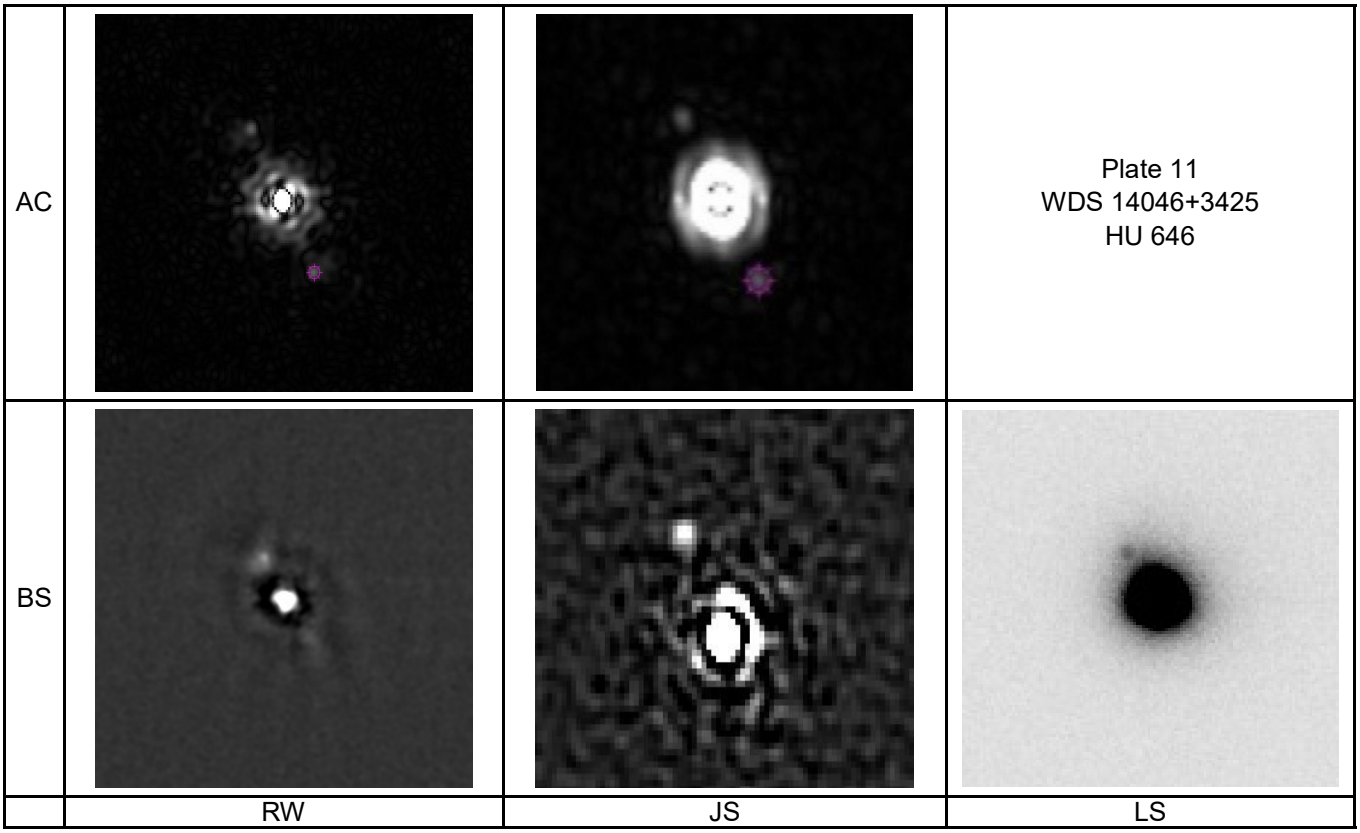

(Continued from page 720)

and bispectrum analysis should facilitate large-scale observational programs that could result in the discovery and subsequent follow-up observations of double stars with faint, late-M companions. This appears to be feasable, and efforts are underway to achieve full automation.

9. Acknowledgements

This research made use of the Washington Double Star Catalog, maintained by the U.S. Naval Observatory, of the REDUC software, developed and maintained by F. Losse, and the Speckle ToolBox software developed by D. Rowe. The authors would like to thank V. Wallen for her careful proof-reading of the final manuscript and R. Harshaw for the very interesting discussions we had throughout the project and his suggestions.

This work has made use of data from the European Space Agency (ESA) mission Gaia (https://www.cosmos.esa.int/gaia), processed by the Gaia Data Processing and Analysis Consortium (DPAC, https://www.cosmos.esa.int/web/gaia/dpac/consortium). Funding for the DPAC has been provided by national institutions, in particular the institutions participating in the Gaia Multilateral Agreement.

10. References

Anderson, J., 1991, "Accurate masses and radii of normal stars", *A & Arv,* **3**, 91.

Dupuy, T., Liu, M., & Ireland, M., 2012, "Testing theory with dynamical masses and orbits of ultracool binaries", ASP Conference Series, in press.

Edward L., Genet, R., Ridgely, J, Rowe, D., Zimmerman, N., "Observation of Large-Delta-Magnitude Close Binaries with Shaped Aperture Masks", 2015, *Journal of Double Star Observations,* **11**, 343.

Foley, E., Genet R., Ridgely J., Rowe D., Zimmerman N., 2015, "Observation of Large Delta Magnitude Close Binaries with Shaped Aperture Masks",

JDSO, 11(1s), pp 343-360.

Harshaw, R., Rowe, D., and Genet, R., 2017, "The Speckle Toolbox: A Powerful Data Reduction Tool for CCD Astrometry", *Journal of Double Star Observations*, **13**, 52-67.

Horch, E.P., Meyer, R.D. and van Altena, W.F., 2014, "Speckle Observations of Binary Stars with the WIYN Telescope-IV-Differential Photometry", *AJ* **127**, 1727-1735.

Kasdin, J., Vanderbei, R., Spergel, D., and M. Littman, 2003, "Extrasolar planet finding via optimal apodized-pupil and shaped-pupil coronographs." *ApJ*, **582**, 1147. http://adsabs.harvard.edu/abs/2003ApJ...582.1147K

Losse, F. Reduc, v5.0, 2017, http://www.astrosurf.com/hfosaf

Mason,D.B., Wycoff G.L., Hartkopf, W.I. Washington Double Star Catalog, 2015. http://www.usno.navy.mil/USNO/astrometry/optical-IR-prod/wds/WDS

Sérot, J., 2015, "Measurements of double stars using a 280 mm reflector and an EM-CCD: 2014-2015 report", *JDSO*, **11**(1s), 361-380.

Sérot, J., 2016a, "Speckle Interferometry of Close Visual Binary Stars with a 280 mm Reflector and an EM -CCD", *JDSO*, **12**(5), pp 488-499.

Sérot, J., 2017, "Measurements of Close Visual Binaries with a 280 mm Reflector and the ASI 290MM Camera", *JDSO*, **13**(2), 268-284.

Sérot, J., 2018a, "Measurements of visual binary stars with M-type companions with a SWIR camera and a 280 mm reflector", *JDSO*, **14**(1), 78-82.

Sérot, J. and Communal, J.E., 2018b, "Measurements of close visual binary stars at the Observatory of Saint-Véran", *JDSO*, **14**(3) 476-486.

Sérot, J., 2018c, "Measurements of Aitken visual binary stars : 2017 report", *JDSO*, **14**(3), 527-537.

Sivaramakrishnan, A., Koresko, C., Makidon, R., Berkefeld, T., & Kuchner, M., 2001, "Ground-based coronography with high-order adaptive optics", *AJ*, **552**, 397.

Singh, G., Martinache, F., Baudoz, P., Guyon, O., Matsuo, T., & Clergeon, C., 2013, "Lyot-based ultra-fine pointing control system for phase mask coronagraphs", *Proceedings of AO4ELTs3 Conference*: Paper 12667.

Vanderbei, R., Spergel, D., & Kasdin, J., 2003, "Spiderweb masks for high-contrast imaging", *AJ*, **590**, 593.

Wasson, R., 2018, "Speckle Interferometry with the OCA Kuhn 22" Telescope", *JDSO*, **14**(2), 223-241.